Alterations of Retinal Vasculature in Cystathionine-Beta-Synthase Mutant Mice, a Model of Hyperhomocysteinemia

Amany Tawfik,[1,2] *Mohamed Al-Shabrawey,*[2–4] *Penny Roon,*[1] *Srinivas Sonne,*[5] *Jason A. Covar,*[1,2] *Surapoon Matragoon,*[2,6] *Preethi S. Ganapathy,*[1,2] *Sally S. Atherton,*[1,2,4] *Azza El-Remessy,*[2,6,7] *Vadivel Ganapathy,*[2,5] *and Sylvia B. Smith*[1,2,4]

Purpose. Mice with moderate/severe hyperhomocysteinemia due to deficiency or absence of the *cbs* gene encoding cystathionine-beta-synthase (CBS) have marked retinal disruption, ganglion cell loss, optic nerve mitochondrial dysfunction, and ERG defects; those with mild hyperhomocysteinemia have delayed retinal morphological/functional phenotype. Excess homocysteine is a risk factor for cardiovascular diseases; however, it is not known whether excess homocysteine alters retinal vasculature.

Methods. *Cbs*$^{+/+}$, *cbs*$^{+/-}$, and *cbs*$^{-/-}$ mice (age ~3 weeks) were subjected to angiography; retinas were harvested for cryosections, flat-mount preparations, or trypsin digestion and subjected to immunofluorescence microscopy to visualize vessels using isolectin-B4, to detect angiogenesis using anti-VEGF and anti-endoglin (anti-CD105) and activated glial cells (anti-glial fibrillary acidic protein [anti-GFAP]) and to investigate the blood–retinal barrier using the tight junction markers zonula occludens-1 (ZO-1) and occludin. Expression of *vegf* was determined by quantitative RT-PCR (qRT-PCR) and immunoblotting. Human retinal endothelial cells (HRECs) were treated with excess homocysteine to analyze permeability.

Results. Angiography revealed vascular leakage in *cbs*$^{-/-}$ mice; immunohistochemical analysis demonstrated vascular patterns consistent with ischemia; isolectin-B4 labeling revealed a capillary-free zone centrally and new vessels with capillary tufts midperipherally. This was associated with increased *vegf* mRNA and protein, CD105, and GFAP in *cbs*$^{-/-}$ retinas concomitant with a marked decrease in ZO-1 and occludin. Homocysteine-treated HRECs showed increased permeability.

Conclusions. Severe elevation of homocysteine in *cbs*$^{-/-}$ mutant mice is accompanied by alterations in retinal vasculature (ischemia, neovascularization, and incompetent blood–retinal barrier). The marked disruption of retinal structure and decreased visual function reported in *cbs*$^{-/-}$ mice may reflect vasculopathy as well as neuropathy. (*Invest Ophthalmol Vis Sci.* 2013;54:939–949) DOI:10.1167/iovs.12-10536

Homocysteine is a sulfur-containing amino acid that is an intermediate in methionine metabolism. Homocysteine is converted to cysteine by the transsulfuration pathway or remethylated to methionine via the remethylation pathway. Decreased rates of homocysteine metabolism through either pathway can lead to excess homocysteine presenting as hyperhomocysteinemia, or in severe cases homocystinuria. Hyperhomocysteinemia is a recognized risk factor for human cardiovascular diseases (e.g., stroke, venous thrombosis) and neurodegenerative diseases.[1] Increased homocysteine has been reported in a broad spectrum of eye-related diseases. For example, ectopia lentis is a major ocular manifestation in homocystinuria.[2] A number of pathological conditions affecting retina have also been linked to hyperhomocysteinemia, such as glaucoma (primary and secondary open-angle glaucoma, exfoliation glaucoma, pigmentary glaucoma),[3–5] macular degeneration, maculopathy and retinal degeneration,[6–8] and diabetic retinopathy.[9,10] Elevated plasma homocysteine is a potential risk factor for the development of premature occlusive atherosclerosis in humans[2]; and clinical investigations provide strong evidence that hyperhomocysteinemia is a risk factor for retinal vascular diseases, including central retinal vein occlusion, branch retinal vein occlusion, and central retinal artery occlusion.[11,12]

To understand the mechanism by which homocysteine affects retina, in vitro and in vivo experimental models have been used. Incubation of the RGC-5 retinal neuronal cell line with 1 mM D,L-homocysteine thiolactone induced apoptotic cell death,[13] and incubation of primary mouse retinal ganglion cells with physiologically relevant levels of this formulation of homocysteine (50 μM) induced significant apoptotic cell death within 24 hours.[14] In vivo studies showed that within 5 days of intravitreal injection of high dosages of D,L-homocysteine thiolactone, marked ganglion cell loss and disruption of the inner retina in mice were observed.[15] Marked loss of photoreceptor cells was observed within 15 days of exposure to high concentrations of D,L-homocysteine thiolactone, and the outer nuclear layer was ablated within 90 days of exposure.[16] The availability of mice lacking the gene encoding cystathionine-beta-synthase (CBS)[17] has permitted analysis of the effects of mild to severe endogenous elevation of homocysteine on retina. Deficiency of CBS, a key enzyme in the transsulfuration pathway, is the most common cause of inherited homocystinuria.[2] Depending upon whether the mouse has one *cbs* allele (*cbs*$^{+/-}$) or no copies of *cbs* (*cbs*$^{-/-}$),

From the Departments of [1]Cellular Biology and Anatomy, [4]Biochemistry and Molecular Biology, [6]Pharmacology and Toxicology, and [7]Ophthalmology, Medical College of Georgia, Georgia Regents University, Augusta, Georgia; the [2]Vision Discovery Institute, Georgia Regents University, Augusta, Georgia; the [3]Department of Oral Biology and Anatomy, College of Dental Medicine, Georgia Regents University, Augusta, Georgia; and [5]Clinical and Experimental Therapeutics, College of Pharmacy, University of Georgia, Augusta, Georgia.

Supported by NIH Grant R01 EY12830 and Georgia Regents University Culver Vision Discovery Institute.

Submitted for publication July 6, 2012; revised November 20 and December 29, 2012; accepted December 30, 2012.

Disclosure: **A. Tawfik**, None; **M. Al-Shabrawey**, None; **P. Roon**, None; **S. Sonne**, None; **J.A. Covar**, None; **S. Matragoon**, None; **P.S. Ganapathy**, None; **S.S. Atherton**, None; **A. El-Remessy**, None; **V. Ganapathy**, None; **S.B. Smith**, None

Corresponding author: Sylvia B. Smith, Department of Cellular Biology and Anatomy, Medical College of Georgia, Georgia Regents University, 1120 15th Street, CB 2901, Augusta, GA 30912-2000; sbsmith@gru.edu.

plasma homocysteine levels range from moderate to severe, respectively. Comprehensive morphological analyses of retinas of mice heterozygous for the *cbs* gene (*cbs*$^{+/-}$), which have an approximately 4- to 7-fold increase in plasma homocysteine and reflect moderate hyperhomocysteinemia, show a mild phenotype characterized by modest cell loss in the ganglion cell layer and decreased thickness of the inner plexiform and nuclear layers.[18] Accompanying the retinal ganglion cell loss are altered mitochondria of the nerve fiber layer and increased expression of the mitochondrial proteins Opa1 and Fis1.[19] Functional studies revealed a gradual reduction of the light and dark amplitudes of the ERG, reduced direct current electroretinography (dc-ERG) light peak, and differences in visual transmission to the visual cortex when visual evoked potentials (VEPs) were recorded.[20]

A much more severe retinal phenotype is observed in mice lacking the gene encoding CBS (*cbs*$^{-/-}$ mice). These mice have an approximately 30-fold increase in plasma homocysteine, an approximately 7-fold increase in retinal homocysteine, and a life span of only ~3 to 5 weeks. The retinas of these mice show hypertrophy of the RPE, loss of cells in the ganglion cell layer, and marked disruption of the inner/outer nuclear retinal layers.[18] Functional studies showed significantly reduced amplitudes of the dark- and light-adapted ERGs in the *cbs*$^{-/-}$ mice and a marked delay in the N1 implicit time determined by recording VEPs.[20]

The data accumulated in hyperhomocysteinemic (*cbs*) mice show clear dysfunction of retinal neurons[18–20]; however, there have been no investigations of the retinal vasculature in these mice. Given the clinical literature demonstrating a strong correlation between hyperhomocysteinemia and retinal occlusive disease, we investigated the vascular phenotype in *cbs*$^{-/-}$ mice as a model of profound hyperhomocysteinemia. Specifically, we used well-established markers to examine retinas for evidence of angiogenesis, reactive gliosis, and altered permeability within the blood–retinal barrier. Our data show that retinas of *cbs*$^{-/-}$ mice manifest these features and may be useful in determining mechanisms of homocysteine-associated retinal vasculopathies.

Materials and Methods

Animals

Information about the generation of mice deficient in *cbs* has been reported previously.[17] Breeding pairs of *cbs*$^{+/-}$ mice (B6.129P2-Cbs^{tm1Unc}/J; Jackson Laboratory, Bar Harbor, ME) were used to establish our colony of *cbs*$^{+/+}$, *cbs*$^{+/-}$, and *cbs*$^{-/-}$ mice. Genotyping, husbandry, and housing conditions for the mice were described in a previous publication.[18] For analysis of retinal vasculature, wild-type (*cbs*$^{+/+}$, $n = 34$), heterozygous (*cbs*$^{+/-}$, $n = 39$), and homozygous mutant (*cbs*$^{-/-}$, $n = 27$) mice were used at ~3 weeks of age, owing to premature death of the homozygous mice. Mean body weights for *cbs*$^{+/+}$ mice (6.84 ± 0.2 g) and *cbs*$^{+/-}$ mice (6.26 ± 0.3 g) did not differ significantly; however, they were significantly greater than for age-matched *cbs*$^{-/-}$ mice (4.53 ± 0.2 g). Experiments were approved by the Institutional Animal Care and Use Committee of Georgia Regents University and adhered to the ARVO Statement for the Use of Animals in Ophthalmic and Vision Research.

Isolectin-B4 Immunostaining in Flat-Mounted Retinal Preparations

To visualize retinal vasculature, eyes were enucleated, fixed in 4% paraformaldehyde overnight, and transferred to PBS. Retinas were dissected, washed with PBS, and incubated with Power Block (BioGenex, San Ramon, CA). They were incubated with the endothelial cell–specific marker biotinylated Griffonia simplicifolia isolectin-B4 overnight at 4°C, followed by incubation with avidin-conjugated Texas Red (Table). Retinas were cut partially at four places along the rim to allow the tissue to be flattened upon Superfrost microscope slides (Fisher Scientific, Pittsburgh, PA). Retinal flat-mount preparations were visualized by immunofluorescence using an Axioplan-2 fluorescent microscope (Carl Zeiss, Göttingen, Germany) equipped with a high-resolution microscope camera. Images were captured and processed using Zeiss Axiovision digital image processing software (version 4.7; Carl Zeiss). To quantify vascularized versus unvascularized (capillary-free) areas of the retinas, we used ImageJ (National Institutes of Health, Bethesda, MD) and outlined the entire retina and then capillary-free areas to obtain a ratio of these values for retinas in each of the mouse groups.

Immunofluorescence of Vascular Markers in Retinal Cryosections

To analyze retinas for new blood vessel formation, evidence of gliosis, and integrity of the blood–retinal barrier, a battery of markers was used. The sources and concentrations of primary and secondary antibodies are provided in the Table. Retinal cryosections were prepared from *cbs*$^{+/+}$, *cbs*$^{+/-}$, and *cbs*$^{-/-}$ mice per our previously described method.[21] Sections were fixed with 4% paraformaldehyde, washed with PBS–Triton X-100, incubated with Power Block (BioGenex), and then incubated with primary antibody for either 3 hours at 37°C or overnight at 4°C; the sections were washed thrice with PBS–Triton X-100 followed by incubation with secondary antibody for 1 hour at 37°C. Sections were washed with PBS–Triton X-100 and coverslipped with Fluoroshield with 4′6-diamidino-2-phenylindole (DAPI) (Sigma Chemical Corp., St. Louis, MO) to label nuclei. Sections were examined by epifluorescence as described above. The intensity of fluorescence was analyzed using Metamorph Image Analysis software (version 6.3; Molecular Devices, Sunnyvale, CA).

Quantitative Reverse-Transcriptase Polymerase Chain Reaction

Neural retinas were isolated from *cbs*$^{+/+}$, *cbs*$^{+/-}$, and *cbs*$^{-/-}$ mice; RNA was extracted per our previously described method.[19] Quantitative real-time PCR was performed using Absolute QPCR SYBR Green Fluorescein Mix (Thermo Scientific, Surrey, UK) and the BioRad iCycler (BioRad, Hercules, CA). The primers used for qPCR were VEGF, upper (CATCTTCAAGCC GTCCTGTGTGC); VEGF, 120-lower (CACCGCCTTGGCTTGTCACATT); and VEGF, 164-lower (GCGGAA CAAGGCTCACAGTGATT). PCR was performed for 40 cycles of 95°C for 30 seconds, 60°C for 30 seconds, and 72°C for 30 seconds; melt curve analysis confirmed the purity of the end products. Resulting C_T values were normalized to 18S and analyzed using the comparative C_T method to obtain fold changes in gene expression.[22]

Immunoblotting to Detect Levels of VEGF and ZO-1

Proteins were extracted from neural retinas isolated from *cbs*$^{+/+}$, *cbs*$^{+/-}$, and *cbs*$^{-/-}$ mice to detect VEGF and zonula occludens-1 (ZO-1) levels according to our published method.[19] Briefly, protein samples were subjected to SDS-PAGE and transferred to nitrocellulose membranes, which were then incubated with mouse monoclonal anti-VEGF antibody (1:500) or a rabbit polyclonal anti-ZO-1 antibody (1:100) at 4°C overnight, followed by a horseradish peroxidase (HRP)-conjugated goat antimouse IgG (1:5000) or goat antirabbit IgG antibody (1:3000). Proteins were visualized with the enhanced chemiluminescence (ECL) Western blot detection system. Membranes were reprobed with mouse monoclonal anti-β-actin antibody (1:5000) as a loading control. Protein levels were quantified as described previously.[19]

Isolation of Retinal Vasculature by Trypsin Digestion

Retinal vessels were isolated per the method of Stitt and colleagues.[23] Briefly, freshly enucleated eyes were fixed with 2% paraformaldehyde overnight. Retinas were dissected, washed in PBS, and incubated while

TABLE. Primary and Secondary Antibodies Used to Analyze Retinal Vasculature

Primary Antibody and Catalog Number	Vendor	Concentration	Use as Marker	Secondary Antibody
Griffonia simplicifolia isolectin-B4 (B-1105)	Vector Labs, Burlingame, CA	7.5 μL/mL	Marker for vessels to detect vessel patterns	Texas Red avidin, 7 μL/mL; Vector Labs
CD105 (endoglin) rat antimouse (lot 75619)	BD Biosciences, San Jose, CA	1:25	Marker for angiogenesis	Alexa Fluor 555 (donkey antirat); Invitrogen, Eugene, OR
VEGF mouse monoclonal IgM (AB 38909)	Abcam Corp., Cambridge, MA	1:250	Marker for angiogenesis	Alexa Fluor 488 (donkey antimouse); Invitrogen, Eugene, OR
GFAP rabbit polyclonal (lot 00019620)	DakoCytomation, Carpenteria, CA	1:100	Marker for stressed Müller cells and astrocytes	Alexa Fluor 488 (goat antirabbit); Invitrogen, Eugene, OR
ZO-1 Rb.PAbzo-1 tight junction (AB 59720)	Abcam, Cambridge, MA	1:250	Marker for cellular tight junctions	Alexa Fluor 488 (donkey antirabbit); Invitrogen, Eugene, OR
Occludin rabbit polyclonal (AB 31721)	Abcam, Cambridge, MA	1:200	Marker for cellular tight junctions	Alexa Fluor 488 (donkey antirabbit); Invitrogen, Eugene, OR
IgM mouse monoclonal (AB 18401)	Abcam, Cambridge, MA	1:200	Isotype control (VEGF study)	Alexa Fluor 488 (donkey antimouse); Invitrogen, Eugene, OR

shaking with 3% crude trypsin in 20 nmol/L Tris buffer, pH 8, at 37°C for 2 hours until vitreous separated from retina. The remaining retinal tissue was soaked in several washes of 5% and 2% Triton X-100 to separate vasculature from the neural retina. The transparent vasculature was visualized using a stereomicroscope and gently flattened onto the microscope slide. After several days of drying, the vasculature was immunostained for isolectin-B4 and occludin and examined by immunofluorescence as described above.

Fluorescein Angiography

To evaluate retinal vasculature and permeability in vivo, $cbs^{+/+}$ and $cbs^{-/-}$ mice were anesthetized using a 20 μL intramuscular injection of rodent anesthesia cocktail (ketamine 100 mg/mL, xylazine 30 mg/mL, acepromazine 10 mg/mL). Pupils were dilated using 1% tropicamide (Bausch and Lomb, Rochester, NY). The mouse was placed on the imaging platform of the Phoenix Micron III retinal imaging microscope (Phoenix Research Laboratories, Pleasanton, CA), and Goniovisc 2.5% (hypromellose; Sigma Pharmaceuticals, LLC, Monticello, IA) was applied liberally to keep the eye moist during imaging. Mice were administered 10 to 20 μL fluorescein sodium (10% Lite) (Apollo Ophthalmics, Newport Beach, CA) (while also receiving Goniovisc 2.5% [hypromellose; Sigma Pharmaceuticals, LLC]), and rapid acquisition of fluorescent images ensued for ~5 minutes.

In Vitro FITC–Dextran Flux Permeability Assay

Human retinal endothelial cells (HRECs) cultured in Complete Classic Medium with culture boost (Cell Systems, Kirkland, WA) were used to evaluate the role of homocysteine in HREC barrier function. HRECs were grown to confluence on fibronectin-coated membranes with 0.4 μm pores (Transwell Corning Costar; Cole-Parmer, Vernon Hills, IL). Culture media was replaced with Serum-Free Medium with RocketFuel (Cell Systems) 2 hours prior to the experiment. To assay the effects of homocysteine on permeability, 50 μM homocysteine thiolactone (Sigma Chemical Corp.) was added to the media of the upper and lower chambers and incubation was carried out for 12 hours, after which time 10 μM FITC-dextran was added to the upper chamber. Control HRECs were supplemented with an equal volume of PBS. After incubation with the FITC-dextran for 6 hours, aliquots from the upper and lower chamber were transferred to a 96-well plate to measure the fluorescence intensity (FI) photometrically using a plate reader (Thermo Scientific Multiskan FC; Fisher Scientific). The ratio FI of the upper chamber to FI of the lower chamber was compared for homocysteine-treated versus control cells. This method to assess permeability was established by Yang et al.[24]

Statistical Analysis

Metamorph quantification of immunofluorescent detection of vascular markers (isolectin-B4, VEGF, glial fibrillary acid protein [GFAP], ZO-1, occludin), data from ImageJ (National Institutes of Health) analysis, and densitometric scans for Western blotting and qPCR were analyzed by Student's *t*-test using the GraphPad Prism software (version 5; GraphPad Software Inc., La Jolla, CA). A P value < 0.05 was considered significant.

RESULTS

Evaluation of Vasculature

Previously reported studies of the retinas of $cbs^{-/-}$ used retinal cryosections to investigate retinal architecture; gross disruption was observed in several retinal layers.[18,20] Examination of retinal sections from $cbs^{-/-}$ mice revealed evidence also of hemorrhage and grossly dilated blood vessels, particularly in the midperipheral area of hematoxylin- and eosin-stained retinal sections (Fig. 1B) compared to the same area of retinal

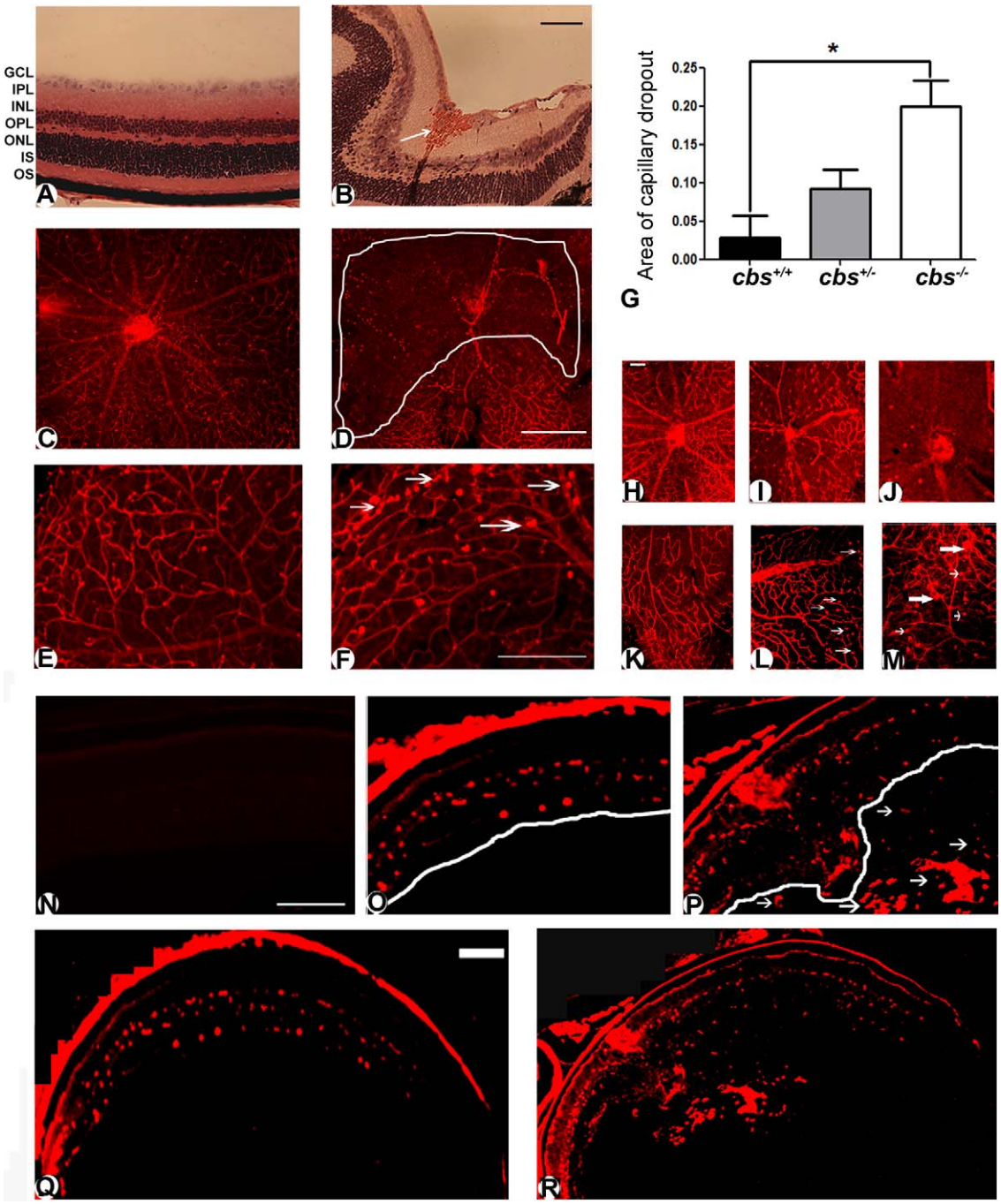

Figure 1. Altered retinal vasculature in $cbs^{-/-}$ mice. Histological assessment of retinal cryosections stained with hematoxylin and eosin (**A**, **B**), showing retinal hemorrhage (*white arrow*) and grossly dilated blood vessels in the $cbs^{-/-}$ retina (**B**) compared to the normal retina of wild-type ($cbs^{+/+}$) mouse (**A**). Retinal flat mounts (**C**–**F**) stained with isolectin-B4 (endothelial cell marker) labeling the retinal vasculature. Retina of $cbs^{-/-}$ mouse shows central capillary dropout (**D**) compared to healthy central vasculature of $cbs^{+/+}$ mouse (**C**). Neovascular tufts (*arrows*) were observed in retinas of $cbs^{-/-}$ mice (**F**), which were not observed in the $cbs^{+/+}$ mouse retina (**E**). Experiments were performed in five mice. *Scale bar*: 40 μm (**B**), 200 μm (**D**, **F**). Morphometric assessment of the central capillary-free areas showed significant increase in $cbs^{-/-}$ retinas compared to wild-type ($cbs^{+/+}$) retinas ([**G**], $^*P < 0.05$, $n = 4$ mice per group). Vasculature of the 3-week-old $cbs^{+/-}$ mice was mildly altered; retinal flat mounts were stained with isolectin-B4 (endothelial cell marker) to label retinal vasculature. (**H**, **K**) $cbs^{+/+}$; (**I**, **L**) $cbs^{+/-}$; (**J**, **M**) $cbs^{-/-}$. There is marked central capillary dropout in the retina of the $cbs^{-/-}$ mouse (**J**) compared to mild dropout in the $cbs^{+/-}$ retina (**I**) and the healthy central vasculature of the $cbs^{+/+}$ mouse (**H**). Neovascular tufts (*large arrows*) and capillary dilations (*small arrows*) were observed in retinas of $cbs^{-/-}$ mice (**M**), which were detected only occasionally in the $cbs^{+/-}$ retina (**L**) and were not observed in the $cbs^{+/+}$ mouse retina (**K**). Experiments were performed in six retinas per group. *Scale bar*: 50 μm. Isolectin-B4–stained frozen sections confirmed the neovascularization in the $cbs^{-/-}$ mouse retinas (**N**–**R**). Retinal cryosections from $cbs^{+/+}$ (**Q**) and $cbs^{-/-}$ (**R**) mice were incubated with isolectin-B4, an endothelial cell–specific marker, to label blood vessels. There were new blood vessels growing into the vitreous in the $cbs^{-/-}$ mice retina, particularly in the midperipheral zone of the retina (**P**), while there were normal vascular patterns in the retina of the wild-type control $cbs^{+/+}$ (**O**). Isolectin-B4 plus galactose (500 mM) was used as an isotype control (**N**). *Scale bar*: 500 μm. GCL, ganglion cell layer; IPL, inner plexiform layer; INL, inner nuclear layer; OPL, outer plexiform layer; ONL, outer nuclear layer; IS/OS, inner/outer segments of photoreceptor cells.

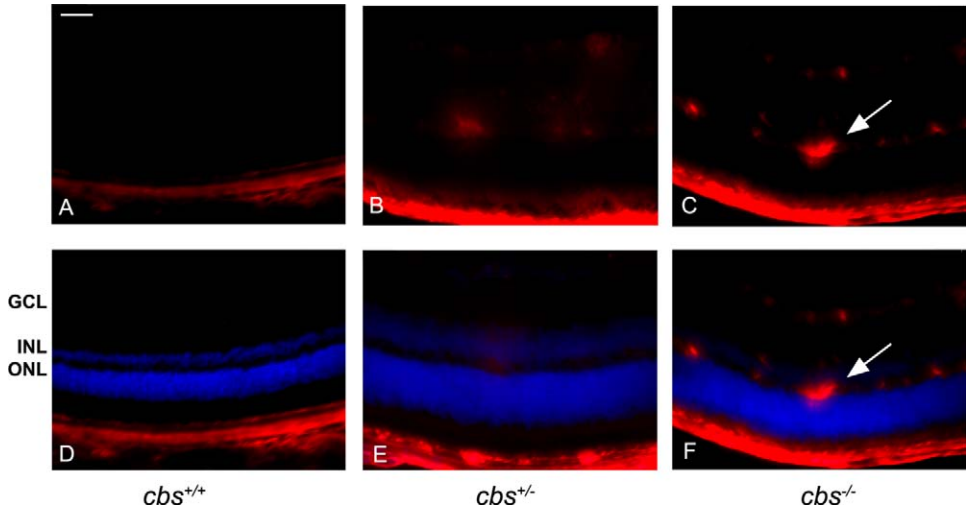

Figure 2. Increased endoglin (CD105) levels in *cbs*$^{-/-}$ mouse retinas. Fluorescent immunodetection of endoglin (*red*), a marker of neovascularization, was performed in retinal cryosections of 3-week-old mice; DAPI (*blue*) was used to label nuclei. Endoglin was minimally detected in *cbs*$^{+/+}$ retinas (**A**, **D**), while endoglin levels were markedly increased in *cbs*$^{-/-}$ retinas (**C**, **F**), particularly in the ganglion cell layer and inner nuclear layer, where the blood vessels are predominant. Occasional endoglin-positive labeling was seen in *cbs*$^{+/-}$ retinas (**B**, **E**). The *arrows* represent neovascularization (new blood vessel formation). *Scale bar*: 50 μm. Experiments were performed in sections from six mice per group. Abbreviations for retinal layers are the same as for Figure 1.

sections of *cbs*$^{+/+}$ mice. Indeed, while the retinas of the *cbs*$^{+/+}$ mice had normal retinal structure and no hemorrhage (Fig. 1A), the retinas of the *cbs*$^{-/-}$ mice did not have a uniform appearance, an observation that confirms earlier findings.[18,20] To further analyze the retinal vasculature, tissues were incubated with isolectin-B4 to label blood vessels in frozen sections and flat-mounted preparations. In retinas of *cbs*$^{+/+}$ mice, multiple arteries branched from the central retinal artery (Fig. 1C). An extensive capillary network was visible between branches. The well-defined branching pattern characteristic of wild-type mice was not observed in the retinas of *cbs*$^{-/-}$ mice (Fig. 1D). A large capillary-free zone is outlined in Figure 1D. Higher magnification of the midperipheral region of the same retinas revealed an intact capillary network in the wild-type (*cbs*$^{+/+}$) mouse (Fig. 1E), with a few capillary tufts as typically observed in young mice; however, there were considerably more capillary tufts in retinas of the *cbs*$^{-/-}$ mouse (Fig. 1F). Collectively, these data suggested ischemia in the central retina of the hyperhomocysteinemic mice and new blood vessel formation in the periphery. We also examined vascular patterns of the heterozygous mice at 3 weeks for comparison to wild-type and homozygous mice. Retinal flat-mount preparations from some of the *cbs*$^{+/-}$ mice showed vascular patterns with mild ischemia (Fig. 1I) compared to preparations in wild type (Fig. 1H), but it was much less severe than in the *cbs*$^{-/-}$ mice (Fig. 1J). There were also a few areas where neovascular tufts were detected in *cbs*$^{+/-}$ mice (Fig. 1L); these were slightly more numerous than in wild type (Fig. 1K) but were not abundant as they were in the retinas of *cbs*$^{-/-}$ mice (Fig. 1M). To quantify the extent of ischemia, we measured the capillary-free zones in the three groups of mice. The analysis revealed a significant increase in the ratio of capillary-free areas to the total retina in *cbs*$^{-/-}$ mice compared to *cbs*$^{+/+}$ mice (Fig. 1G).

Using isolectin-B4 staining in frozen sections, we observed neovascularization in the *cbs*$^{-/-}$ mice; in some animals, blood vessels projected into the vitreous particularly in the midperipheral area. Figure 1Q shows a low magnification of the wild-type retina labeled with isolectin-B4, and Figure 1O provides a higher magnification showing the evenly distributed endothelial cells within the retina. In contrast, Figure 1R shows low magnification of the *cbs*$^{-/-}$ retina with evidence of isolectin-B4 labeling not only in the retina, but also within the vitreous. Higher magnification of this pathology is shown in Figure 1P. In studies in which the isolectin-B4 was omitted (negative control) or when 500 mM galactose was used with the isolectin-B4 (isotype control), no signal was detected, reflecting the specificity of the reaction; data are shown for the isotype control (Fig. 1N). Arrows point to the extensive new blood vessels observed in the vitreous of these mutant mice.

Assessment of Angiogenesis

Endoglin (CD105) is a proliferation-associated and hypoxia-inducible protein abundantly expressed in angiogenic endothelial cells[25,26]; it is used as a marker for new blood vessels. To investigate new blood vessel formation in the moderately (*cbs*$^{+/-}$) and severely (*cbs*$^{-/-}$) hyperhomocysteinemic mice, endoglin levels were analyzed by immunofluorescence in retinal cryosections (Fig. 2). The upper panels show the red fluorescence labeling endoglin only, and the lower panels present merged images with DAPI (blue) to allow localization within the retinal nuclear layers. Endoglin was not detected in the neural retinas of *cbs*$^{+/+}$ mice (Figs. 2A, 2D). In retinas of *cbs*$^{+/-}$ mice, endoglin was faintly detected in the midretinal region (Figs. 2B, 2E), whereas in retinas of cbs$^{-/-}$ mice, endoglin was detected in multiple retinal layers including the ganglion cell and inner nuclear layers (Figs. 2C, 2F). These data provide evidence of angiogenic activity in retinas of the *cbs*$^{-/-}$ mice.

To confirm neovascularization in retinas of *cbs*$^{-/-}$ mice, experiments to detect vascular endothelial growth factor (VEGF) were performed. VEGF is a 17 kD dimeric glycoprotein that is a potent endothelial cell mitogen. It stimulates proliferation, migration, and tube formation leading to angiogenic growth of new blood vessels.[27] Immunofluorescent detection of VEGF in retinal cryosections revealed low levels in *cbs*$^{+/+}$ retinas, a mild increase in retinas of *cbs*$^{+/-}$ mice, and a dramatic increase in the *cbs*$^{-/-}$ mice (Fig. 3A). The data were obtained using a fluorescence microscope in which the exposure time of the camera was held constant. In studies in which the primary antibody was omitted (negative control) or when IgM was used in place of the primary antibody (isotype

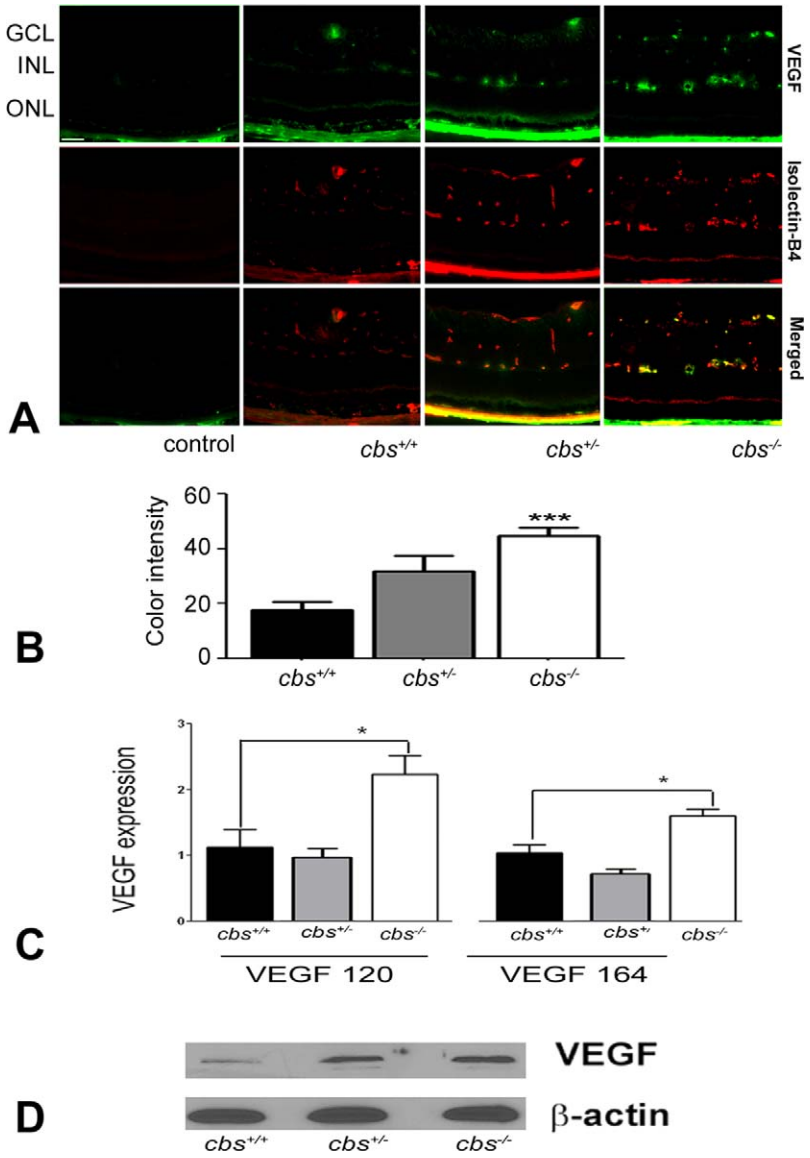

Figure 3. Increased VEGF levels in $cbs^{-/-}$ mouse retinas. (**A**) Fluorescent immunodetection of VEGF (*green*), a marker of neovascularization, and isolectin-B4 (*red*), a marker of endothelial cells, was performed in retinal cryosections from 3-week $cbs^{+/+}$, $cbs^{+/-}$, and $cbs^{-/-}$ mice. The *far left panel* provides controls: an isotype (IgM) control for VEGF and a negative control (omission of the primary antibody), but with inclusion of the secondary antibody, for isolectin-B4. *Scale bar*: 50 μm. Abbreviations for retinal layers are the same as for Figure 1. (**B**) Quantification of the intensity levels of VEGF immunofluorescence, showing significantly greater VEGF levels in $cbs^{-/-}$ compared to $cbs^{+/+}$ and $cbs^{+/-}$ mice ($^{***}P < 0.001$, $n = 6$). (**C**) Expression of VEGF mRNA is increased in neural retinas of $cbs^{-/-}$ mice compared to $cbs^{+/-}$ and $cbs^{+/+}$ mice. Fold change in expression of $vegf_{120}$ and $vegf_{164}$ was determined by quantitative RT-PCR ($^{*}P < 0.05$). (**D**) Representative immunoblot to detect VEGF in retinas of $cbs^{+/+}$ mice compared with $cbs^{+/-}$ and $cbs^{-/-}$ mice. Protein was extracted from retina and subjected to SDS-PAGE; immunoblotting was performed with an affinity-purified antibody against VEGF 164 and subsequently with an antibody against β-actin (internal loading control).

control), no signal was detected (Fig. 3A). Metamorph analysis of sections of three independent experiments indicated an approximately 2-fold increase in VEGF levels in the $cbs^{-/-}$ retinas (Fig. 3B). To investigate whether the genes encoding various forms of VEGF were altered in the retinas of the $cbs^{-/-}$ mice compared to $cbs^{+/-}$ or $cbs^{+/+}$, quantitative RT-PCR (qRT-PCR) was performed using primers specific for $VEGF_{120}$ and $VEGF_{164}$. In humans there are multiple forms of VEGF; in mice, there are three isoforms ($VEGF_{120}$, $VEGF_{164}$, $VEGF_{188}$). We examined the first two isoforms, as they are most prominent and are associated with angiogenesis.[27] qRT-PCR analysis revealed a significant increase in expression of both $vegf_{120}$ and $vegf_{164}$ in the $cbs^{-/-}$ mice (Fig. 3C). Immunoblotting to detect the level of VEGF protein demonstrated a marked increase in VEGF levels when normalized to β-actin (loading control) in the $cbs^{+/-}$ and $cbs^{-/-}$ mice compared with $cbs^{+/+}$ retinas (Fig. 3D). Taken collectively, the data from studies of endoglin and VEGF support new blood vessel formation in the retinas of hyperhomocysteinemic mice.

Evidence of Reactive Gliosis

The data suggesting that retinas of $cbs^{-/-}$ mice were ischemic (Fig. 1), which in turn induced new blood vessel formation (Figs. 1–3), prompted investigation of glial fibrillary acid protein (GFAP), a 54 kD intermediate filament protein that is a major constituent of astrocytes. GFAP levels were investigated by immunofluorescence in retinal cryosections (Fig. 4A)

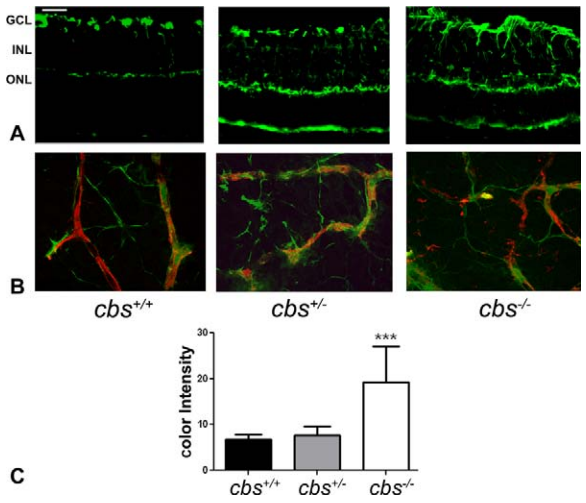

Figure 4. Increased GFAP expression in *cbs*$^{-/-}$ mouse retina. GFAP levels were detected by immunofluorescence in retinal cryosections and flat-mount preparations. (**A**) Retinal cryosections of 3-week *cbs*$^{+/+}$, *cbs*$^{+/-}$, and *cbs*$^{-/-}$ mice that were incubated with an antibody against GFAP followed by incubation with Alexa Fluor 488 (*green*)–labeled secondary antibody, showing increase in GFAP immune reactivity in both astrocytes and Müller cells in the *cbs*$^{-/-}$ retina compared to wild-type control *cbs*$^{+/+}$, where GFAP is expressed in astrocytes only. (**B**) Retinal flat-mount preparations from *cbs*$^{+/+}$, *cbs*$^{+/-}$, and *cbs*$^{-/-}$ mice immunostained for isolectin-B4 (*red*) to visualize vasculature and GFAP (*green*), showing altered vasculature and ragged appearance of the astrocytes in *cbs*$^{-/-}$ mice compared to normal-shaped vasculature and astrocytes in the wild-type control *cbs*$^{+/+}$ ($n = 6$). *Scale bar*: 50 μm. (**C**) Quantification of the data obtained from metamorphic analysis of color intensity of GFAP (significantly greater than wild-type, $^{***}P < 0.001$, $n = 6$).

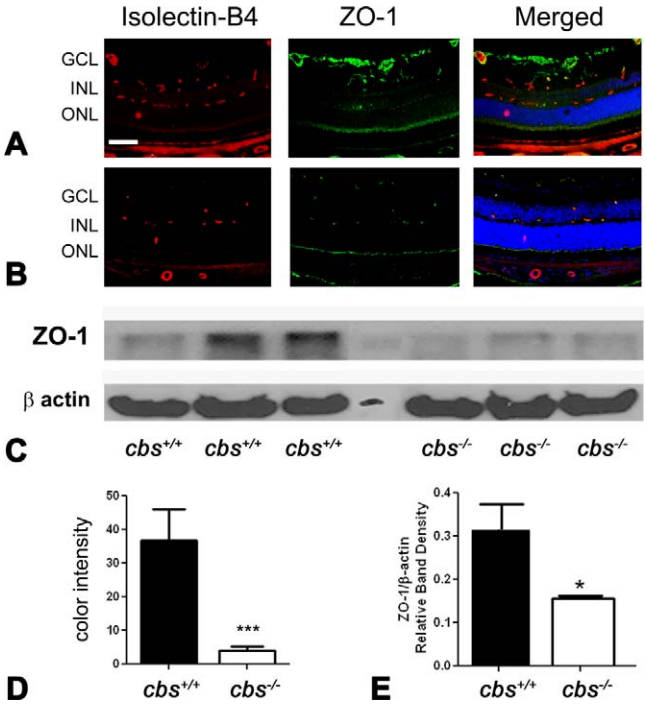

Figure 5. Decreased ZO-1 levels in *cbs*$^{-/-}$ mouse retina. Retinal cryosections from (**A**) *cbs*$^{+/+}$ and (**B**) *cbs*$^{-/-}$ mice were incubated with an antibody against ZO-1 (*green*), a marker of tight junctions, and isolectin-B4 (*red*) to label blood vessels. *Scale bar*: 40 μm; abbreviations for retinal layers are the same as for Figure 1. (**C**) Retinal protein was extracted and subjected to SDS-PAGE, followed by immunoblotting to detect Z0-1 (molecular weight ([M_r] = 198 kD); β-actin was used as the loading control. (**D**) Quantification of immunohistochemical fluorescence intensity ($^{***}P < 0.001$, $n = 6$). (**E**) Quantification of densitometric scans of protein bands shown in (**C**) ($^{*}P < 0.05$).

and flat-mount preparations (Fig. 4B) from *cbs*$^{+/+}$, *cbs*$^{+/-}$, and *cbs*$^{-/-}$ mice. Under normal conditions, Müller cells contain low levels of GFAP; however, GFAP expression is strongly upregulated under a variety of conditions including retinal degeneration, retinal detachment, and ischemia.[28] Significantly higher levels of GFAP were detected in retinal cryosections of *cbs*$^{-/-}$ mice compared with wild-type mice (Fig. 4A). While the astrocytes in the vicinity of the ganglion cell layer were positive in the *cbs*$^{+/+}$ mice and low-level GFAP was present in the outer plexiform layer, the labeling was not excessive; however, in the *cbs*$^{-/-}$ mice, GFAP levels increased dramatically. Labeling of the Müller cell radial fibers was quite prominent in *cbs*$^{-/-}$ mice (Fig. 4A). GFAP labeling of *cbs*$^{+/-}$ mouse retina increased slightly, though not significantly, compared to wild type. The quantification of these data is presented in Figure 4C. GFAP labeling was investigated also in flat-mount preparations using isolectin-B4 to find out whether GFAP colocalized with retinal blood vessels; GFAP also labels astrocytes or activated Müller cells. In the *cbs*$^{+/+}$ retinas, GFAP-positive astrocytes are evident; they have a normal star-shaped appearance. A few astrocytes are labeled that are ensheathing well-organized blood vessels (Fig. 4B). In contrast, in the *cbs*$^{-/-}$ retinas there are more GFAP-labeled glia, which have more diffuse branching patterns and a ragged appearance. In addition, while the glial cells are associated with the isolectin-B4–labeled vessels, the vessels are disrupted (Fig. 4B). The increased GFAP levels in retinas of *cbs*$^{-/-}$ mice are consistent with the ischemia observed and likely reflect reactive gliosis in this hyperhomocysteinemic model. With respect to the GFAP–isolectin-B4 labeling in retinas of heterozygous mice, there was a modest increase in GFAP labeling in *cbs*$^{+/+}$ retinas compared to wild type, which was less than observed in age-matched homozygous (*cbs*$^{-/-}$) mice.

Examination of Inner Blood–Retinal Barrier Proteins

Newly formed blood vessels are often immature and leaky.[29] The data showing new blood vessel formation in retinas of *cbs*$^{-/-}$ mice (Figs. 1, 2), coupled with increased expression of VEGF (Fig. 3), prompted investigation of markers for an intact blood–retinal barrier. Maintenance of the blood–retinal barrier is essential for retinal homeostasis. The tight junction proteins ZO-1 and occludin contribute to the retinal permeability barrier and are present in endothelial and epithelial cells.[29]

ZO-1 levels were investigated by immunofluorescence in retinal cryosections. Significantly lower levels of ZO-1 were detected in retinas of *cbs*$^{-/-}$ mice (Fig. 5) compared with wild-type *cbs*$^{+/+}$ animals (Fig. 5A). The immunofluorescence levels were quantified, and the data reflect the significant decrease in ZO-1 levels (Fig. 5D). To confirm the decrease in ZO-1 levels determined by immunohistochemical methods, retinas were harvested from additional *cbs*$^{+/+}$ and *cbs*$^{-/-}$ mice, and protein was isolated and subjected to immunoblotting to detect ZO-1. There was a marked decrease in ZO-1 in the *cbs*$^{-/-}$ retinas compared to *cbs*$^{+/+}$ mice (Fig. 5C); the densitometric quantification of the data is shown in Figure 5E.

Expression of occludin was also investigated in retinas of *cbs*$^{-/-}$ mice compared to *cbs*$^{+/+}$ mice. Retinal cryosections were incubated with antibodies against occludin and isolectin-B4. In the *cbs*$^{+/+}$ retinas, occludin was detected in several

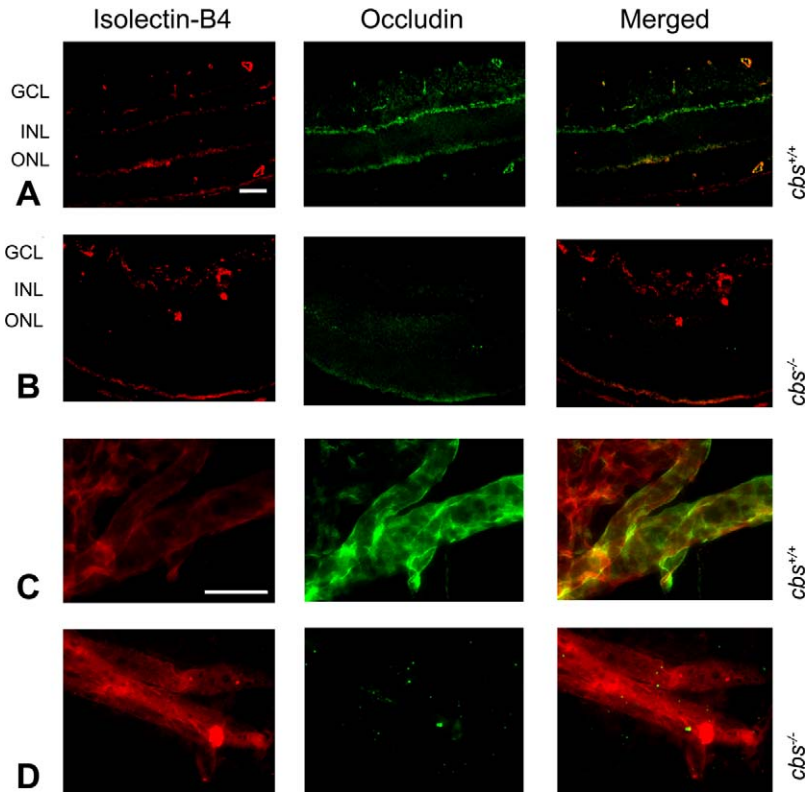

Figure 6. Occludin expression in mouse retina. Retinal cryosections of eyes from *cbs*$^{+/+}$ and *cbs*$^{-/-}$ mice, incubated with antibodies against occludin and isolectin-B4 followed by incubation with Alexa Fluor 488 (*green*)- and Texas Red avidin (*red*)-labeled secondary antibodies, show decreased occludin immune reactivity in the *cbs*$^{-/-}$ retina (**B**) compared to wild-type *cbs*$^{+/+}$ (**A**). Trypsin-digested retina, immunostained for isolectin-B4 (*red*) and occludin (*green*), show decreased occludin expression in *cbs*$^{-/-}$ retina (**D**) compared to *cbs*$^{+/+}$ (**C**). *Scale bar*: 50 μm (**A**, **B**), 20 μm (**C**, **D**).

retinal layers (Fig. 6A, middle panel) and colocalized in many regions with isolectin-B4 (Fig. 6A, merged panel), whereas in the *cbs*$^{-/-}$ retinas the level of occludin was markedly decreased (Fig. 6B, middle and merged panels). Additional retinas were digested with trypsin to permit visualization of blood vessels and were subsequently subjected to dual-labeling immunohistochemical methods to detect occludin and isolectin-B4. The isolectin-B4 clearly labeled blood vessels in the *cbs*$^{+/+}$ retina (Fig. 6C, left panel); there was considerable detection of occludin in these vessels (Fig. 6D, middle and merged panels). The trypsin digestion method revealed blood vessels in the *cbs*$^{-/-}$ retina (Fig. 6D, left panel); however, the occludin in these retinas was sparse (Fig. 6C, middle and merged panels). Indeed, levels were extremely low throughout the retinas, consistent with the minimal labeling observed in the cryosections (Fig. 6B).

In Vivo Fluorescein Angiography and In Vitro Assessment of Permeability

The decrease in the levels of the two tight junction proteins suggests compromised integrity of the blood–retinal barrier. To investigate this further in vivo, we subjected *cbs*$^{+/+}$ and *cbs*$^{-/-}$ mice to fluorescein angiography. The images were taken in the same phase/time in both wild type and knockout (KO) after fluorescein administration. Images were collected immediately after fluorescein administration, then every minute for 5 minutes. After capturing, the images were arranged according to the capture time; then cbs$^{+/+}$ and cbs$^{-/-}$ images were compared in the same time points. The *cbs*$^{+/+}$ showed normal filling of retinal blood vessels with fluorescein and no observable leakage of fluorescence into the surrounding area (Fig. 7A, left panel), reflecting an intact blood–retinal barrier in these animals. In contrast, when the *cbs*$^{-/-}$ mice were subjected to fluorescein angiography, hyperfluorescence was observed (Fig. 7A, right panel). That is, the vessels were less well defined, and a diffuse fluorescence was observed in surrounding retinal tissue after 2 minutes of fluorescein administration. These data suggest that the blood–retinal barrier is compromised in these mice.

In addition to the in vivo studies, we conducted an in vitro experiment in which we analyzed the effects of excess homocysteine on the permeability of endothelial cells. HRECs were used in this analysis and allowed to grow on the filter in the upper chamber of a transwell plate. The cells were treated with homocysteine for 12 hours and then were incubated with a fluorescent reagent (FITC-dextran), which allows analysis of the portion of fluoresce that leaks from the upper to the lower chamber. In cells treated with PBS (control), a low level of FITC was detected in the lower chamber; however, the level of fluorescence increased significantly when the cells were incubated with homocysteine (Fig. 7B). The data suggest that at least in vitro, hyperhomocysteinemia can alter endothelial cell barrier function.

Discussion

The present study provides compelling evidence that severe hyperhomocysteinemia is associated with alteration of retinal vasculature, including ischemia concomitant with neovascularization. Using young mice that lack a key enzyme in the transsulfuration pathway, cystathionine-beta-synthase, we have observed retinal hemorrhage; central capillary dropout and midperipheral new blood vessel formation; increased retinal

levels of biological markers of angiogenesis (CD105 and VEGF); increased expression of GFAP in astrocytes and Müller cells consistent with reactive gliosis; decreased levels of the tight junction proteins ZO-1 and occludin; and fluorescein angiography consistent with vascular leakage and a defective blood–retinal barrier.

While this study represents the first systematic investigation of the retinal vasculature in the *cbs*$^{-/-}$ mutant mouse, there are a number of reports of severe vasculopathy in other tissues of this mutant mouse model. For example, experimental application of endothelium-dependent vasodilators to large arteries, such as the aorta and the carotid artery, revealed a decreased dilatory response compared to that in vessels isolated from control animals.[30] Morphological changes have been observed in the large vessel walls, including increased thickness and hypertrophy.[31] It is noteworthy that studies of hindlimb vessels in the *cbs*$^{+/-}$ mice demonstrated impaired angiogenesis, while our studies of retinal vasculature in the *cbs*$^{-/-}$ mice revealed increased expression of markers of angiogenesis.[32] Interestingly, there have been reports of increased blood–brain barrier permeability,[33] which may be important in the development of small vessel disease and dementia. These observations are consistent with our findings of decreased expression of tight junction proteins in the retinal vessels of *cbs*$^{-/-}$ mice, which would reflect disruption of the blood–retinal barrier.

In the present study, we focused on homozygous mice 3 weeks of age and compared the data to those for age-matched heterozygous and wild-type mice. The rationale behind this experimental age is that the homozygous *cbs* mice have a severely shortened life span and do not live beyond ~5 weeks.[17] *cbs*$^{-/-}$ mice represent the most severe form of hyperhomocysteinemia and can be considered a model of the human disease homocystinuria. This disease is due to homozygous deficiency of CBS and occurs in ~1 of 300,000 births. The most prominent clinical features in these patients are premature arteriosclerosis, thromboembolism, mental retardation, ectopia lentis, hepatosteatosis, and skeletal abnormalities.[34] Regarding visual complications, there have been reports in this patient population of glaucoma, optic neuropathy, and myopia and even cases of no light perception.[35–37] Thus the visual phenotype for these patients is severe. Our studies with the *cbs*$^{-/-}$ mice reflect a similar severe retinal phenotype. Our earlier electrophysiological assessment of these mutants revealed profound loss of visual function characterized by significant reductions in the a- and b-waves of the electroretinogram, as well as abnormal retinal output to the visual cortex shown by marked delay in VEP implicit time[20] and disruption of the inner and outer retina.[18,20]

In the current work, our examination of vasculature revealed marked ischemia, new blood vessel formation, and impairment of the blood–retinal barrier. We detected an increase in the expression of VEGF, which frequently accompanies new blood vessel formation. Interestingly, during development, hyperhomocysteinemia leads to impaired early extra-embryonic vascular development by altering composition of the vascular beds, as well as reduced expression of VEGF-A and VEGFR-2.[38] It has also been reported that homocysteine alters endothelial cell function, including endothelial cell proliferation, which is closely related to angiogenesis. However, the direct relationship between homocysteine and angiogenesis is unknown. In the current study, we hypothesize that severe hyperhomocysteinemia, due to deletion of *cbs,* may lead to impairment of retinal vascular development causing retinal ischemia, which later on stimulates new blood vessel formation from existing blood vessels (angiogenesis). However, this hypothesis requires rigorous experimentation and mechanistic studies if it is to be validated.

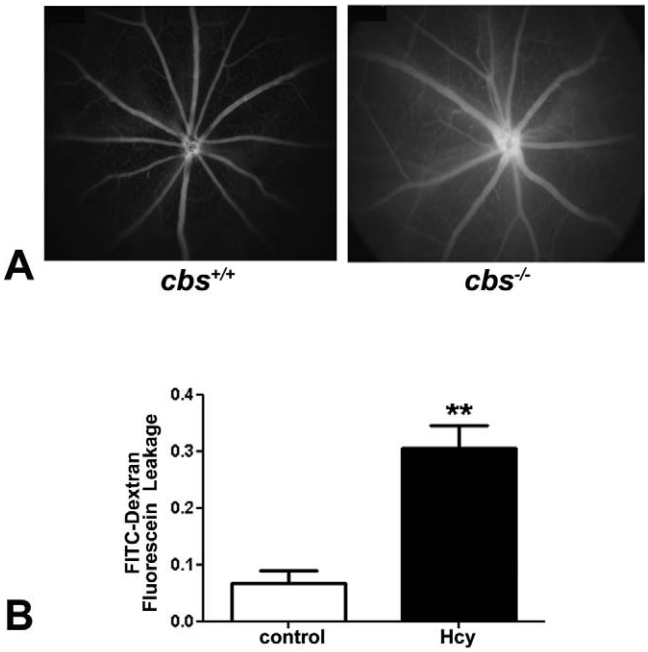

Figure 7. In vivo and in vitro assessment of blood–retinal barrier function. (**A**) Data from fluorescein angiography, performed to evaluate the retinal vasculature and to determine whether permeability was altered in living mice (in vivo experiment). *Left panel* shows a representative angiogram of a *cbs*$^{+/+}$ mouse; *right panel* shows an angiogram of a *cbs*$^{-/-}$ mouse. Data are representative of five mice studied in each group. (**B**) Data from an FITC–dextran flux permeability assay performed using HRECs in the absence (control) or presence of 50 μM homocysteine. Fluorescence intensity measured in the lower chamber versus the upper chamber of the transwell plate was determined photometrically, and the ratio of these values was significantly higher in homocysteine-treated HRECs versus PBS-incubated cells ($^{**}P < 0.01$, $n = 3$).

The findings of this study present an intriguing conundrum: Does homocysteine induce disruption of retinal vasculature, or is it merely a biomarker of disrupted vasculature? The data presented herein support the notion that excess levels of homocysteine may be deleterious to retinal vasculature. It is important to bear in mind, however, that the hyperhomocysteinemia investigated here is due to a lack of CBS. CBS irreversibly converts homocysteine to cystathionine via the transsulfuration pathway leading to the formation of cysteine, which can be converted to three very important biochemical products: glutathione (GSH), a key antioxidant; hydrogen sulfide (H_2S), a critical signaling molecule that plays a pivotal role in vascular and neurological homeostasis[39,40]; and taurine, the most abundant amino acid in retina. Hence, our observations of disrupted retinal vasculature in *cbs* mutant mice (and retinal neuronal death reported earlier[18–20]) may be due to excess homocysteine, or they may be due to decreased levels of these downstream factors critical for retinal health. Future experiments will analyze these downstream factors in this mouse model. Additionally, it is fortuitous that there are other genetic models in which homocysteine is elevated in the presence of an intact transsulfuration pathway. For example, mice deficient in (or lacking) the enzyme methylene tetrahydrofolate reductase (MTHFR), which converts N_5,N_{10}-methylenetetrahydrofolate into N_5-methyltetrahydrofolate, the predominant circulating form of folate in the body, have high levels of homocysteine but no defect in the transsulfuration pathway.[41] These mice offer a handsome alternative tool for examining the consequences of excess homocysteine in the

retina. With these mice in hand, we should be poised to dissect the role of hyperhomocysteinemia in retinal structure and function; studies are now under way to investigate this systematically.

Acknowledgments

We thank Cory Williams for excellent care of our mouse colony.

References

1. Perła-Kaján J, Twardowski T, Jakubowski H. Mechanisms of homocysteine toxicity in humans. *Amino Acids*. 2007;32:561–572.
2. Mudd SH. Hypermethioninemias of genetic and non-genetic origin: a review. *Am J Med Genet C Semin Med Genet*. 2011; 157:3–32.
3. Bleich S, Jünemann A, Von Ahsen N, et al. Homocysteine and risk of open-angle glaucoma. *J Neural Transm*. 2002;109: 1499–1504.
4. Vessani RM, Ritch R, Liebmann JM, Jofe M. Plasma homocysteine is elevated in patients with exfoliation syndrome. *Am J Ophthalmol*. 2003;136:41–46.
5. Jaksic V, Markovic V, Milenkovic S, Stefanovic I, Jakovic N, Knezevic M. MTHFR C677T homozygous mutation in a patient with pigmentary glaucoma and central retinal vein occlusion. *Ophthalmic Res*. 2010;43:193–196.
6. Axer-Siegel R, Bourla D, Ehrlich R, et al. Association of neovascular age-related macular degeneration and hyperhomocysteinemia. *Am J Ophthalmol*. 2004;137:84–89.
7. Seddon JM, Gensler G, Klein ML, Milton RC. Evaluation of plasma homocysteine and risk of age-related macular degeneration. *Am J Ophthalmol*. 2006;141:201–203.
8. Tsina EK, Marsden DL, Hansen RM, Fulton AB. Maculopathy and retinal degeneration in cobalamin C methylmalonic aciduria and homocystinuria. *Arch Ophthalmol*. 2005;123: 1143–1146.
9. Aydemir O, Türkçüoğlu P, Güler M, et al. Plasma and vitreous homocysteine concentrations in patients with proliferative diabetic retinopathy. *Retina*. 2008;28:741–743.
10. Yang G, Lu J, Pan C. The impact of plasma homocysteine level on development of retinopathy in type 2 diabetes mellitus. *Zhonghua Nei Ke Za Zhi*. 2002;41:34–38.
11. Semba RD. Retinal vascular disease. In: *Nutrition and Health: Handbook of Nutrition and Ophthalmology.* Totowa, NY: Humana Press; 2007:257–280.
12. Lahey JM, Kearney JJ, Tunc M. Hypercoagulable states and central retinal vein occlusion. *Curr Opin Pulm Med*. 2003;9: 385–392.
13. Dun Y, Thangaraju M, Prasad P, Ganapathy V, Smith SB. Prevention of excitotoxicity in primary retinal ganglion cells by (+)-pentazocine, a sigma receptor-1-specific ligand. *Invest Ophthamol Vis Sci*. 2007;48:4785–4794.
14. Ganapathy PS, Dun Y, Ha Y, et al. Sensitivity of staurosporine-induced differentiated RGC-5 cells to homocysteine. *Curr Eye Res*. 2010;35:80–90.
15. Moore P, El-sherbeny A, Roon P, Schoenlein PV, Ganapathy V, Smith SB. Apoptotic cell death in the mouse retinal ganglion cell layer is induced in vivo by the excitatory amino acid homocysteine. *Exp Eye Res*. 2001;73:45–57.
16. Chang HH, Lin DP, Chen YS, et al. Intravitreal homocysteine-thiolactone injection leads to the degeneration of multiple retinal cells, including photoreceptors. *Mol Vis*. 2011;17: 1946–1956.
17. Watanabe M, Osada J, Aratani Y, Kluckman K, Reddick R, Malinow MR. Mice deficient in cystathionine beta-synthase: animal models for mild and severe homocysteinemia. *Proc Natl Acad Sci. U S A*. 1995;92:1585–1589.
18. Ganapathy PS, Moister B, Roon P. Endogenous elevation of homocysteine induces retinal neuron death in the cystathionine-beta-synthase mutant mouse. *Invest Ophthalmol Vis Sci*. 2009;50:4460–4470.
19. Ganapathy PS, Perry RL, Tawfik A. Homocysteine-mediated modulation of mitochondrial dynamics in retinal ganglion cells. *Invest Ophthalmol Vis Sci*. 2011;52:5551–5558.
20. Yu M, Sturgill-Short G, Ganapathy P, Tawfik A, Peachey NS, Smith SB. Age-related changes in visual function in cystathionine-beta-synthase mutant mice, a model of hyperhomocysteinemia. *Exp Eye Res*. 2012;96:124–131.
21. Ha Y, Saul A, Tawfik A. Late-onset inner retinal dysfunction in mice lacking sigma receptor 1 (σR1). *Invest Ophthalmol Vis Sci*. 2011;52:7749–7760.
22. Schmittgen TD, Livak KJ. Analyzing real-time PCR data by the comparative C(T) method. *Nat Protoc*. 2008;3:1101–1108.
23. Stitt AW, Li YM, et al. Advanced glycation end products (AGEs) co-localize with AGE receptors in the retinal vasculature of diabetic and of AGE-infused rats. *Am J Pathol*. 1997;150:523–531.
24. Yang J, Duh EJ, Caldwell RB, Behzadian MA. Antipermeability function of PEDF involves blockade of the MAP kinase/GSK/beta-catenin signaling pathway and uPAR expression. *Invest Ophthalmol Vis Sci*. 2010;51:3273–3280.
25. Fonsatti E, Sigalotti L, Arslan P, Altomonte M, Maio M. Emerging role of endoglin (CD105) as a marker of angiogenesis with clinical potential in human malignancies. *Curr Cancer Drug Targets*. 2003;3:427–432.
26. Nassiri F, Cusimano MD, Scheithauer BW, et al. Endoglin (CD105): a review of its role in angiogenesis and tumor diagnosis, progression and therapy. *Anticancer Res*. 2011;31: 2283–2290.
27. Penn JS, Madan A, Caldwell RB, Bartoli M, Caldwell RW, Hartnett ME. Vascular endothelial growth factor in eye disease. *Prog Retina Eye Res*. 2008;27:331–371.
28. Lewis GP, Fisher SK. Up-regulation of glial fibrillary acidic protein in response to retinal injury: its potential role in glial remodeling and a comparison to vimentin expression. *Int Rev Cytol*. 2003;230:263–290.
29. Erickson KK, Sundstrom JM, Antonetti DA. Vascular permeability in ocular disease and the role of tight junctions. *Angiogenesis*. 2007;10:103–117.
30. Jiang X, Yang F, Tan H, et al. Hyperhomocystinemia impairs endothelial function and eNOS activity via PKC activation. *Arterioscler Thromb Vasc Biol*. 2005;25:2515–2521.
31. Baumbach GL, Sigmund CD, Bottiglieri T, Lentz SR. Structure of cerebral arterioles in cystathionine β-synthase-deficient mice. *Circ Res*. 2002;91:931–937.
32. Bosch-Marce M, Pola R, Wecker AB, et al. Hyperhomocyst(e)inemia impairs angiogenesis in a murine model of limb ischemia. *Vasc Med*. 2005;10:15–22.
33. Kamath AF, Chauhan AK, Kisucka J, et al. Elevated levels of homocysteine compromise blood-brain barrier integrity in mice. *Blood*. 2006;107:591–593.
34. Mudd SH, Skovby F, Levy HL, et al. The natural history of homocystinuria due to cystathionine β-synthase deficiency. *Am J Hum Genet*. 1985;37:1–31.
35. Andersson HC, Marble M, Shapira E. Long-term outcome in treated combined methylmalonic acidemia and homocystinemia. *Genet Med*. 1999;1:146–150.
36. Taylor RH, Burke J, O'Keefe M, Beighi B, Naughton E. Ophthalmic abnormalities in homocystinuria: the value of screening. *Eye (Lond)*. 1998;12:427–430.

37. Juszko J, Kubalska J, Kanigowska K. Ocular problems in children with homocystinuria. *Klin Oczna*. 1994;96:212–215.
38. Oosterbaan AM, Steegers EA, Ursem NT. The effects of homocysteine and folic acid on angiogenesis and VEGF expression during chicken vascular development. *Microvasc Res*. 2012;83:98–104.
39. Beard RS Jr, Bearden SE. Vascular complications of cystathionine β-synthase deficiency: future directions for homocysteine-to-hydrogen sulfide research. *Am J Physiol Heart Circ Physiol*. 2011;300:H13–26.
40. Whiteman M, Le Trionnaire S, Chopra M, Fox B, Whatmore J. Emerging role of hydrogen sulfide in health and disease: critical appraisal of biomarkers and pharmacological tools. *Clin Sci (Lond)*. 2011;121:459–488.
41. Lawrance AK, Racine J, Deng L, Wang X, Lachapelle P, Rozen R. Complete deficiency of methylenetetrahydrofolate reductase in mice is associated with impaired retinal function and variable mortality, hematological profiles, and reproductive outcomes. *J Inherit Metab Dis*. 2011;34:147–157.